PROCEEDINGS B

royalsocietypublishing.org/rspb

Research

Cite this article: Vankelst M, Fischer V, Michaud M, Tamagnini D, Pollock TI, Meloro C, Tseng ZJ, Chatar N. 2026 Decoupling geometry and topography reveals contrasting ecomorphological signals in carnivoran carnassial teeth. *Proc. R. Soc. B* **293**: 20260400.
https://doi.org/10.1098/rspb.2026.0400

Received: 13 February 2026
Accepted: 16 June 2026

Subject Category:
Morphology and biomechanics

Subject Areas:
ecology, evolution, theoretical biology

Keywords:
diet, carnivora, geometric morphometrics, topography, carnassial teeth, convergence

Author for correspondence:
Melvin Vankelst
e-mail: melvin.vankelst@uliege.be

Supplementary material is available online at https://doi.org/10.6084/m9.figshare.c.8555994.

THE ROYAL SOCIETY PUBLISHING

Decoupling geometry and topography reveals contrasting ecomorphological signals in carnivoran carnassial teeth

Melvin Vankelst[1,2], Valentin Fischer[1], Margot Michaud[1,3], Davide Tamagnini[4], Tahlia I. Pollock[5], Carlo Meloro[6], Z. Jack Tseng[7] and Narimane Chatar[7,8]

[1]Evolution & Diversity Dynamics Lab, UR Geology, Université de Liège, Liège, 4000, Belgium
[2]Directorate Earth and History of Life, Royal Belgian Institute of Natural Sciences, Brussels, Belgium
[3]Institut Polytechnique UniLaSalle, Université d'Artois, Mont-Saint-Aignan, 73130, France
[4]Department of Biology and Biotechnologies "Charles Darwin", Sapienza University of Rome, Roma, 00185, Italy
[5]Palaeobiology Research Group, University of Bristol, Bristol, BS8 1TH, UK
[6]Research Centre in Evolutionary Anthropology and Palaeoecology, School of Biological & Environmental Sciences, Liverpool John Moores University, Liverpool, L3 5UX, UK
[7]Functional Anatomy and Vertebrate Evolution Lab, Department of Integrative Biology University of California Berkeley, Berkeley, 94720, USA
[8]Departamento de Ecología y Geología, Facultad de Ciencias, Universidad de Málaga, Málaga, 29071, Spain

MV, 0009-0003-3048-2100; VF, 0000-0002-8808-6747; MM, 0000-0001-7075-9862; CM, 0000-0003-0175-1706; ZJT, 0000-0001-5335-4230

The lower carnassial tooth (m1) is a key innovation underlying the ecological diversification of Carnivora. However, their exceptionally diverse phenotypes result from both functional adaptation and phylogenetic inertia which challenges ecomorphological inferences. We investigate patterns of morphological convergence in the carnassial teeth of 142 extant carnivoran species spanning all terrestrial families and major dietary strategies. We compare the performance of occlusal topographic metrics (Relief Index, Dirichlet Normal Energy, and Orientation Patch Count rotated) and high-density three-dimensional geometric morphometrics (HD3DGM) in distinguishing ecomorphological signal at high taxonomic level, a key element of large-scale diversity analyses. Our results show that HD3DGM recovers a stronger and more consistent dietary signal than topographic metrics, particularly across dissimilar morphologies and at higher taxonomic levels. Within omnivory, insectivory and frugivory, species sharing the same dietary strategies exhibit clear patterns consistent with morphological convergence in the geometric data, while it is only true for frugivory when using topographic metrics. We show that many-to-one topography behaviour weakens the quality of ecomorphological inference at higher taxonomic scales. Our results reframe the context in which each method is most appropriately applied.

1. Introduction

Among the numerous physiological and anatomical singularities of mammals, the complexity and diversity of their dentition are of particular interest; in addition to a generally pronounced heterodonty and diphyodont development, the interspecific morphological diversity of dental crowns is also unique among vertebrates [1,2]. This wide variety of dental shapes can be used to infer taxonomic identity [3,4] but is also indicative of diet and feeding strategies [2,5,6]. In this regard, mammalian molars, especially lower molars, are often studied for the strong dietary signal they are thought to retain [7,8]. Among extant placental mammals, Carnivora is the only clade to have

evolved a distinctive, blade-like first lower molar. Together with the upper P4, they are referred to as the 'carnassial complex'—a defining trait of their order. This morphology is associated with masticatory behaviour such as slicing through flesh and tendons and is often regarded as a key element in understanding their evolutionary success [4,9,10]. From the hypercarnivorous lion to the herbivorous giant panda, carnivorans have achieved a dietary diversity known in few other mammalian orders [11]. Macroevolutionary transitions into such a wide variety of niches are associated with secondary modifications in the morphology of their carnassial teeth such as bicuspid architecture in felids or simplification towards a conical shape in pinnipeds [12] leading to an extensive diversity of shapes.

There are two main approaches to quantifying tooth crown phenotype in mammals: (i) geometric morphometrics, describing the shape of the crowns by extracting cartesian coordinates from collections of individual landmarks and semi-landmarks [13]; and (ii) topography of the occlusal surface that distills information about the complexity and anisotropy of those teeth. The general geometry of carnassial teeth can be variable among species of the same family, yet many exhibit a clear phylogenetic signal that usually allows unambiguous taxonomic identification as well as dietary classification [4,9,14–16]. As topographic tools have been shown to reliably recover diet in multiple mammalian clades such as rodents, primates and carnivorans [7,9,17,18], it can be hypothesized that greater morphological convergence would be found in occlusal topography than in tooth geometry among taxa sharing similar diets. However, this hypothesis is based on localized analyses made on intra-generic or intra-familial taxa that may respond differently than analyses made at higher scales.

While several authors have discussed the morphological convergences—and divergences—between extant and extinct clades [17,19–26], no study to our knowledge, has thoroughly investigated the question of multi-level adaptation in carnivoran carnassial tooth anatomy in relation to diet. Such large-scale quantitative analysis needs to be conducted in extant taxa with established dietary preferences, so that future analogous application in the fossil record beneficiates from ecomorphological validation. In this study, we focus on the lower carnassial tooth (m1) to investigate whether geometry and occlusal topography each capture synergistic versus conflicting ecomorphological signals in extant carnivorans. By combining high-density geometric morphometrics, topographic analyses and phylogenetic comparative methods, we address two main questions: (i) what signals do geometric and occlusal topographic features convey about ecomorphological traits? and (ii) which shape-describing method best reflects trophic ecology among modern carnivorans? Finally, we present theoretical insights into these approaches and discuss their associated challenges and opportunities in order to define their ideal scope of application.

2. Material and methods

(a) Morphological dataset

We gathered a dataset of three-dimensional models of lower carnassials from 142 extant carnivoran species, representing 52% of recorded species when excluding pinnipeds [27]. Because of their particular ecological niche and dental morphology (exhibiting almost homodont post-canine morphology), pinnipeds are not considered in this study (see the electronic supplementary material, S1 for complete list of specimens). All 13 terrestrial families of carnivorans are sampled and, of the 108 genera recognized by Burgin *et al*. [27], 92 are present in our dataset (85%). The mean body mass of each species was obtained from the CarniFOSS database [28].

(b) Phylogeny and taxonomy

To assess the phylogenetic signal in the geometry and topography of the lower m1, we used the time-scaled total evidence phylogeny of carnivoramorphans from Faurby *et al*. [29]. We generated a single tree, based on all 1000 trees contained in the *appex1.nex* file by following a maximum clade credibility approach using the 'maxCladeCred' function from the *phangorn* package [30]. We then pruned it to match the species in our dataset and renamed the tips to follow the most recent taxonomical considerations.

(c) Diets

Extant carnivorans were classified into diet categories modified from Van Valkenburgh [4]. We used multiple types of dietary data present in the literature such as stomach and scat content as well as feeding observations. The categories are established based on percentage of biomass intake or, if not available, feeding occurrence. A complete list of the references used for dietary attribution can be found in the electronic supplementary material S1. The categories are as follows:

(i) hypercarnivorous: greater than 80% of vertebrates (muscle, organs or bones of vertebrates);
(ii) mesocarnivorous: 80–50% of vertebrates;
(iii) piscivorous: greater than 50% fish;
(iv) insectivorous: greater than 50% land invertebrates;
(v) omnivorous: less than 80% plants and less than 50% vertebrate flesh or invertebrates;
(vi) herbivorous: greater than 80% plants;
(vii) frugivorous: greater than 80% fruits, honey, or nectar
(viii) molluscivorous: greater than 50% of molluscs, crustaceans and echinoderms.

Though sometimes approximative considering that species may exhibit geographical and/or temporal variability in their diet, these categories fit well for capturing dominant dietary trends. Additionally, we created an index to categorize the carnivory

level of each species. It classifies species based on the proportion of vertebrate flesh matter in their diet. Following the diet categories previously established, frugivorous and herbivorous taxa were classified as level 0, omnivorous, insectivorous and molluscivorous taxa, who occasionally prey on vertebrates, as level 1 and piscivorous, meso- and hypercarnivorous as level 2. As diet was not sufficiently documented for 13 out of the 142 species (see the electronic supplementary material, S11); analyses relying on the diet were performed on a subset of 129 taxa. Accordingly, level 3 reflects the species whose diet is not sufficiently known and were excluded from such analyses.

(d) Model acquisition and scanning

Lower carnassial three-dimensional meshes were obtained via surface digitization, computed tomography (CT)-scan reconstructions or downloaded from MorphoSource (see the electronic supplementary material S1). Most of the specimens digitized for this project were scanned using the Artec Space Spider three-dimensional scanner (three-dimensional point accuracy of 50 µm and three-dimensional resolution of 100 µm). Meshes recovered from scans conducted by colleagues or external institutions were obtained using surface, medical and CT scanners. Owing to the variety of technologies used, the resolution of the meshes obtained varies. To avoid biases, resolution-sensitive analyses were performed on standardized meshes (see §2g). Similarly, because centroid size could not always be recovered from our scans, the body mass was used instead as the size estimator. Information relative to model processing can be found in the electronic supplementary material.

(e) High-density three-dimensional geometric morphometrics

Every carnassial model was initially landmarked with anchoring points using Landmark v. 3.0.0.6. Our method consists of 12 fixed landmarks on the surface of the crown. The complete protocol can be found in the electronic supplementary material, figure S1. After the placement of the fixed landmarks, 4000 surface pseudolandmarks [31] were automatically generated on the surface of the three-dimensional template in R using a protocol modified from Fischer *et al*. [32]. First, we placed the same 12 fixed landmarks as in our carnassials dataset on a template. An idealized *Vulpavus* sp. (stem carnivoramorphan) left lower molar model was chosen to serve as a general template (see figure 1), with the idealization process consisting of a smoothing step followed by a straightening of the edge of the tooth to dissipate any possible circumvoluted base. Then, the point clouds forming the mesh of the template is homogenized through geodesic distance maximization sampling by using the *vcgSample* function [33] with *geodes = TRUE*. Afterwards, the *fastKmeans* function [33] is used to generate *n* number of equidistant surface pseudolandmarks depending on the desired precision of anatomical sampling (i.e. 4000 in this study). Following this, the template with the 12 fixed landmarks and the 4000 generated pseudolandmarks were combined in the 'createAtlas' function of the 'Morpho' package in R to create an atlas (see figure 1). These points were then projected on each specimen using the *placePatch* function of the *Morpho* package [33] as described by Fischer *et al*. [32] (see figure 1) with the fixed landmarks acting as anchors for the positioning of the projected pseudolandmarks. All data treatment and analyses were made on the RStudio interface (R v. 4.5.1).

(f) Generalized Procrustes and principal component analyses

A generalized Procrustes analysis (GPA) was applied on the whole set of three-dimensional coordinates (4012 points per specimen) using the *gpagen* function of the *geomorph* package [34] with the semi-landmarks defined as sliders through the 'surface' argument of the *gpagen* function. The Procrustes coordinates from the GPA were then subjected to a principal component analysis (PCA) using the *gm.prcomp* function from *geomorph* to represent the main axes of variation in carnassial shape and construct the morphospace. Computation cost and requirements can be found in the electronic supplementary material, S3.

(g) Topographic and crown complexity analyses

To conduct occlusal surface analyses on each species without including resolution or defect biases, all three-dimensional meshes were standardized following this routine: (i) orientation of the occlusal plane as positively following the *z*-axis in Wrap Geomagic; (ii) minor 'Taubin' smoothing (1 iter) using vcgSmooth; (iii) cutting of the base using the *plyPlaneCut* function; and (iv) standardization of the mesh to 8000 vertices with *vcgQEdecim*. All these functions were drawn from the Rvcg package [33]. Then, using the molaR package in RStudio [35], we calculated three metrics describing occlusal complexity and topography (hereafter referred to as 'topographic data'): the Relief Index (RFI), the Orientation Patch Count rotated (OPCr) and the Dirichlet Normal Energy (DNE). Together, these three metrics are the most common dental topography metrics used to reconstruct diet. The RFI is a scalar obtained by dividing the three-dimensional surface of a model by its two-dimensional imprint from an occlusal perspective, following Boyer [31]. The RFI is indicative of the overall elevation profile of the tooth and carries a significant dietary signal in primates [36]. We used 'findAlpha = TRUE' for 137 species out of 142 resulting in a common alpha of 1. As 'findAlpha' could not recover an effective value by itself for the remaining five species, we tested several values and chose an alpha of 0.5 to ensure precise definition of the base. The OPCr is a scalar determined by compiling patches of a mesh surface that share general orientation and sums the number of unique patches iteratively after rotating mesh a selected number of degrees around the *z*-axis [17,35]. It is usually regarded as a good indicator of the proportion of meat ingested, with hypercarnivorous taxa exhibiting the lowest values to fully herbivorous taxa exhibiting the highest values [17]. The function was

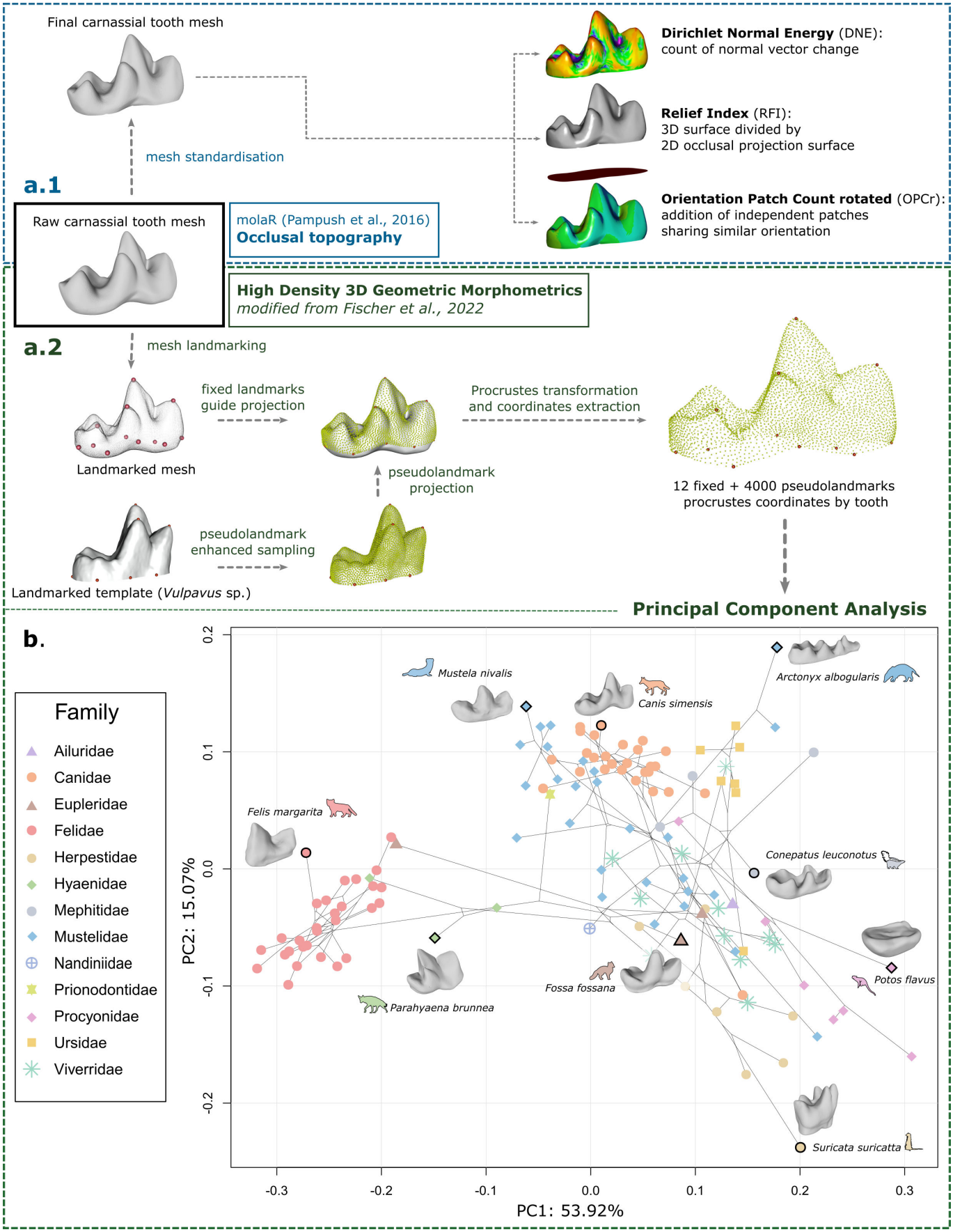

Figure 1. Workflow for topographic and geometric analyses: (a.1) topographic and occlusal complexity protocol (a.2) high-density three-dimensional geometric morphometrics modified from [32], and (b) phylomorphospace. Silhouettes from www.phylopic.org.

used with the following standard argument set-up '*steps = 8, step size = 5.625, minimum faces = 3, minimum area = 0*'. The DNE is a scalar that is calculated by counting changes in normal vectors of a surface to characterize its curvature and was shown to be a good indicator of diet in euarchontans, while also being less methodologically sensitive than OPCr [36]. For DNE, outliers were excluded separately within convex and concave regions to avoid bias from extreme sharpness in one curvature class using the

oex = 's' argument. To conserve as much information as possible, the discard boundary argument of the same function was set up as 'Leg', so that only vertices which have a segment on the edge were disregarded.

(h) Phylogenetic generalized least squared analyses

To explore the relationship between diet and topography, we used phylogenetic generalized least square (PGLS) methods against diet and the carnivory index (0-2). We used *mvgls* from the 'mvMORPH' package [37] and compared several models (Brownian Motion, Ornstein Uhlenbeck, lambda…), iteratively. The body mass of each species was also added as an explicative variable of the model log_{10}(*body mass*), with and without assuming interaction between topography and body mass. We then selected the best model by inspecting the Akaike information criterion values. After adjusting the model with *mvgls*, we followed with a *manova.gls* [37] to test it. For both *mvgls* analyses based on dietary categories, the lambda model fitted best, without interaction between topographic/geometric metrics and body mass. For the *mvgls* analyses explained by *carnivory level* (0-2) and body mass, the lambda model with interaction between *carnivory level* and log_{10}(*body mass*) fitted the best in topographic data, while the lambda model without interaction was better supported in geometric data. The manova.gls analyses were followed by an effect size estimate through the *effectsize* function of the 'mvMORPH' package [37]. Tests and results are reported in the electronic supplementary material, S3.

(i) Geometric and topographic disparity analysis

To investigate geometric (Procrustes coordinates from high density three-dimensional geometric *morphometrics* (HD3DGM)) and topographic (RFI, DNE and OPCr) disparity, we used the function dispRity from the homonym package [38]. Within each family (electronic supplementary material, figure S2) and dietary category, disparity was quantified as the mean variance of Procrustes coordinates or topographic metrics calculated across species. Given the high taxonomic coverage of the dataset, these analyses were conducted to estimate realized extant disparity across families and dietary categories rather than to perform null-hypothesis significance testing. Disparity values are therefore reported as descriptive point estimates and interpreted in light of group sample sizes. To account for the potential contribution of body mass-related variance, reflecting allometric scaling, we repeated the analyses on residuals of regressions of shape or topographic metrics against log_{10}-transformed body mass. This was performed using the *procD.lm* function from the *geomorph* package [34] for Procrustes coordinates, and the standard *lm* function from *stats* for OPCr, DNE and RFI metrics. Because the three topographic metrics differ in magnitude, each was first standardized (*z*-scores), and residuals were computed separately. Residuals from the three metrics were then combined into a single matrix and analysed using *dispRity* following the same procedure as for geometric data.

(j) Convergence analyses

To test for the presence of morphological convergences between species within the same diet category, we used the *search.conv* function (RRphylo package) developed by Castiglione *et al*. [19] on both topographical and geometrical data. Results of this function when investigated 'within state' (i.e. search for convergence between species sharing a similar trait) contains four metrics: (i) θ: the mean angle (in degrees) between the phenotypic vectors of all pairwise species comparisons within the state. The angle can vary from 0° to 180°, reflecting the similarity of the variables (close to 0° meaning high resemblance, while values close to 180° indicating oppositional phenotypes); (ii) *p*: the *p*-value associated with this angle; (iii) θ_{time}: a value corresponding to the mean angle between the species belonging to the state divided by the mean phylogenetic distance among these species; and (iv) p_{time}: the *p*-value associated with θ_{time} estimated by permutation. Ultimately, p_{time} corresponds to the proportion of randomly generated species-groups that exhibit a convergence signal equal or superior to the one observed in the studied state. Just as for the disparity analyses, we also tested how allometry (based on body mass) impacts convergence signals (see the electronic supplementary material, tables S1 and S2). Therefore, we first performed the search.conv analyses on the data obtained through PCA of the Procrustes coordinates, then performed the same PCA analysis on the residuals of the linear model exploring body mass explained variance, similarly as for the disparity analysis. However, we used a phylogenetic approach in this model as we assumed that the impact of body mass on dental change may be different depending on taxa. Therefore, we used *ProcD.pgls* [34] for geometric data as it is designed to be robust against multivariate and interdependent data. For the independent topographic data, we substitute it by the *phylolm* function [39]. In both analyses, the conventional PCA and the PCA on residuals, we kept the first 16 principal components (PCs) to reduce the number of dimensions and consequent instability while maintaining ≈95% of explained variance (95.17% for raw geometric data and 94.99% for mass free geometric data). Topographic data were standardized before analysis. The *search.conv* function does not test convergence *sensu stricto* but identifies cases of phenotypic similarity exceeding Brownian expectations given phylogenetic distance [40]. Significant θ values therefore indicate either convergent evolution, parallelism or evolutionary conservatism. Only when θ_{time} is also significant can similarity be interpreted as unlikely to result solely from shared ancestry. In our analyses, we used the 'declusterization' argument to minimize the impact of closely related species on the retrieved signal. Consequently, although search.conv does not formally demonstrate reduction of phenotypic distance through time, our results do identify patterns consistent with convergence. Additionally, because some diet categories have relatively few species (e.g. $n = 4$ for molluscivorous and herbivorous), we used a high number of permutations (i.e. nsim = rsim = 9999) to reduce Monte-Carlo error and ensure stable estimation of permutation-based *p*-values.

(k) Phylogenetic signal analysis

To recover the phylogenetic signal of the geometric and topographic data, we used the *physignal* function from the Geomorph package [34] with 999 iterations. We used it separately on the Procrustes coordinates and on the vector combining the three topographic metrics.

3. Results

(a) Phylomorphospace

The phylomorphospace (figure 1) resulting from the first two PCs (PC1 = 53.92%, PC2 = 15.07%) reveals two main zones of occupation. PC1 is mainly driven by the relative development of the talonid, which is reduced in lower values and more developed in higher values, whereas PC2 is driven by the aspect ratio, with low values being associated with compact morphologies. The first zone corresponds to a dense cluster in the negative values of PC1 and PC2 and is occupied almost exclusively by felids, reflecting a highly derived and constrained bicuspid morphology. The second zone is wider; spanning the whole PC2 values while restricted to higher values of PC1. Within this region, canids appear quite constrained, whereas other families such as mustelids and euplerids occupy a wider area; even though the latter are represented by a limited number of specimens (n = 5). The highest values on PC1, corresponding to the stronger development of the talonid, are found in procyonids followed by mephitids, herpestids and badgers. The lowest values on PC2 are mostly observed in herpestids. Finally, two regions of the morphospace are sparsely occupied among sampled modern carnivorans; those correspond to the lowest values of PC1 with extreme values on PC2 (lower and upper left corners), suggesting that both morphologies are absent in extant taxa.

(b) Phylogenetic least squares

PGLS analyses demonstrated notable differences between fine scale three-dimensional geometric and occlusal topographic metrics. First, when dietary categories were used, diet better explained geometry (ξ^2 = 0.218, $p << 0.01$) than it explained topography (ξ^2 = 0.054, $p << 0.01$). Despite this, $\log_{10}$(body mass) remains a stronger predictor of morphology for both geometry (ξ^2 = 0.3163, $p << 0.01$) and topography (ξ^2 = 0.157, $p << 0.01$). Replacing dietary categories with carnivory level substantially improved trophic explanatory power, particularly for topographical data. Carnivory level explained 14.1% of topographical variance ($p << 0.01$), representing a near threefold increase compared with diet-based models, while $\log_{10}$(body mass) accounted for a comparable proportion of variance (14.2%, $p << 0.01$). A significant interaction between carnivory level and body mass was detected for topography (ξ^2 = 0.068, p = 0.034), indicating that the effect of carnivory level varies across body mass scales. For geometric data, carnivory level also explained a greater proportion of variance than diet (31.39%, $p << 0.01$), though no significant interaction with body mass was supported. Log_{10}(body mass) remained a slightly stronger predictor of geometric variation, explaining 31.5% of the variance ($p << 0.01$). Detailed statistical outputs are provided in the electronic supplementary material.

(c) Disparity by diet

Our disparity analyses do not recover the same relative ranking between geometry and topography. In the latter, insectivorous taxa exhibit the highest disparity, with a low allometry impact. Molluscivorous, omnivorous and frugivorous species show rather similar values although the disparity of molluscivorous taxa drops when accounting for the body mass-explained variance while it increases for frugivorous species. Geometry-wise, the highest-ranking diet (frugivory) and the lowest-ranking diet (herbivory) are separated by a comparatively small margin. Insectivorous species' geometrical disparity remains high with limited body mass explained variation. Hypercarnivorous taxa exhibit a much larger morphological range in geometry than in topography. Overall, insectivory seems to be associated with a high disparity regardless of method, while herbivory is the diet associated with the lowest disparity (figure 2), although this might be notably biased by its small sample size (n = 4).

(d) Convergence

(i) Geometric convergence

We recovered a phylogenetic signal of K_{mult} = 0.787 (p = 0.0001) in our Procrustes coordinates, indicating rather stable morphology within clades. Multiple diets are associated with a pattern consistent with convergence (significant p-value for both the theta angle, $p(\theta)$, and the theta angle divided by patristic distance, $p(\theta_{\text{time}})$; table 1, table 2). The value of θ and θ_{time} quantifies, respectively, the strength of the phenotypic similarity, with values ranging from 0° (parallel phenotypic vector) to 180° (opposed phenotypic vector), and the rate of convergence in degrees by patristic distance unit, here in degrees per million years. Among the eight diets in our dataset, three were recovered as exhibiting geometric convergence: insectivory, omnivory and frugivory with a fourth, hypercarnivory, falling just beyond. The rather small theta angle between the seven frugivorous species of

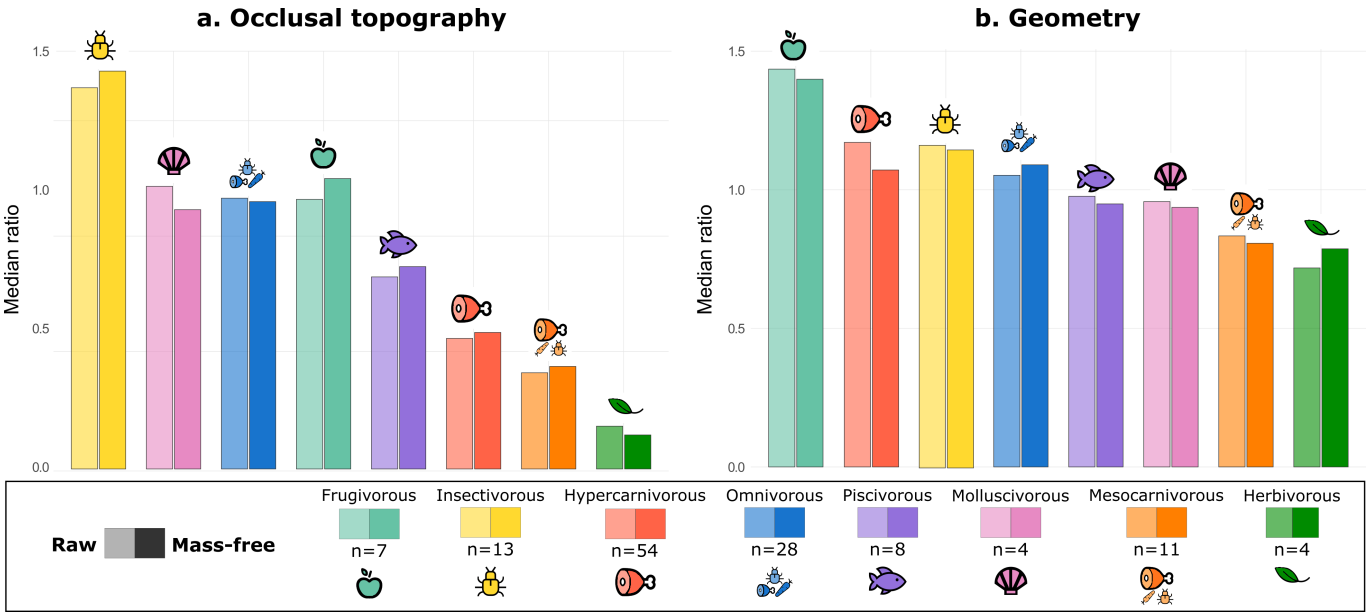

Figure 2. Disparity (mean of variance) by diet ranked from highest to lowest, with (right) and without (left) body mass explained variance suppression. (a) Topographical and occlusal complexity metrics disparity median ratio. (b) Geometrical metrics disparity median ratio.

our dataset (60.76°; p_{FDR} = 0.01) suggests high phenotypic resemblance between those species. Moreover, when accounting for phylogenetic relationships, the signal is significant ($p_{time\ FDR}$= 0.001). Frugivory is also associated with the largest mean temporal distance between species (i.e. 90.49 Myr), resulting in a convergence rate of 0.677° Myr^{-1}. Insectivorous taxa (n = 13) have an even smaller theta of 58.39° (p_{FDR} = 0.002) with a significant convergence signal ($p_{time\ FDR}$ = 0.003). Similarly, the convergence rate between insectivorous taxa is equal to 0.802° Myr^{-1} with average distance of 77.33 Myr. Omnivory also conveys a highly significant convergence signal in the geometry of their carnassial teeth though their raw resemblance is lower than in previous cases with a theta angle of 68.89° (p_{FDR} = 0.0008; $p_{time\ FDR}$= 0.001). Despite this, the convergence rate observed in omnivorous species is higher than in insectivorous and frugivorous taxa with a value of 0.929° Myr^{-1} (mean distance = 86.67 Myr). Hypercarnivorous species show a weaker general resemblance with each other, returning a theta angle of 76.50° (p_{FDR} = 0.035) but exceed the 0.5 threshold for convergence ($p_{time\ FDR}$ = 0.0804). Every other diet category, except for piscivory (p_{FDR} = 0.1120), shows some degree of anatomical similarity though no convergence is detected when theta is divided by the patristic distance. Herbivory, for instance, produced the lowest θ angle (θ = 48.475°, p_{FDR} = 0. 0194), but convergence is not supported ($p_{time\ FDR}$ = 0.875).

(ii) Topographic convergence

The vector combining standardized topographical and occlusal complexity metrics (RFI, DNE and OPCr) recovers a relatively low phylogenetic signal indicating strong lability ($K_{Bloomberg}$ = 0.307, p = 0.0001). However, only one diet was associated with a significant signal when the patristic distance is considered. This signal is found in frugivorous species with a rather small phenotypic angle of 58.91° ($p_{ang\ FDR}$ = 0.0386) and is accompanied by a rate of convergence of 0.669° Myr^{-1} ($p_{time\ FDR}$ = 0.045). Other significant phenotypic resemblances are detected; omnivorous species exhibit topographic similarity (θ = 79.835°, $p_{ang\ FDR}$ = 0.0240) but as $p_{FDR}(\theta_{time})$ is not significant (0.958), parallelism or conservatism is likely. Herbivorous species who exhibit the strongest phenotypic similarity (θ = 17.925°, $p_{ang\ FDR}$ = 0.0064) slightly exceed the commonly accepted significant p-value of 0.05 when Benjamini–Hochberg adjustments are made ($p_{time\ FDR}$ = 0.0582).

4. Discussion

(a) Decoupling topographic and geometric methods

In our analyses, we find notable differences in convergence results between topographic and geometric data, both with and without accounting for the variance related to body mass. In geometry, seven out of eight dietary categories were observed as phenotypically similar (p-value < 0.05), while only three were recovered as such in topography. This correlates with the substantially stronger phylogenetic signal observed in geometry (K_{mult} = 0.79) than in topography (K_{mult} = 0.307). The three-dimensional configuration of carnassial teeth is indeed strongly linked with their taxonomic identity, which is also not independent of dietary preferences. Because most families exhibit marked specialization towards specific diets or trophic level, dietary classes do not represent a balanced sample of family-level diversity but instead consist of subsets of specific families or genera. At high taxonomic scale and for carnivorans, values that represent what appears to be more labile/less constrained traits (e.g. topographic data) can therefore be less predictive of trophic niche than traits that experience stronger phyletic inertia. Additionally, differences between raw and body mass-free results are often negligible in geometric convergence analyses

Table 1. Search.conv 'within state' on geometric data. (θ represents the average phenotypic angle between species sharing the same dietary category. θ_{time} corresponds to the angular distance divided by the patristic distance between species. p indicates p-value, p_{FDR} refers to Benjamini–Hochberg adjusted p-values.)

diet category	n	θ	$p(\theta)$	$p_{FDR}(\theta)$	θ_{time}	$p(\theta_{time})$	$p_{FDR}(\theta_{time})$
frugivorous	7	60.764	0.0037	0.0098	0.678	0.0002	0.0012
herbivorous	4	48.475	0.0097	0.0194	1.275	0.8745	0.8746
hypercarnivorous	54	76.500	0.0307	0.0350	0.937	0.0402	0.0804
insectivorous	13	58.393	0.0005	0.0020	0.802	0.0011	0.0029
mesocarnivorous	11	71.829	0.0148	0.0197	1.007	0.2098	0.3244
molluscivorous	4	53.068	0.0145	0.0197	0.956	0.2433	0.3244
omnivorous	28	68.887	0.0001	0.0008	0.929	0.0003	0.0012
piscivorous	8	77.634	0.1104	0.1104	1.060	0.4741	0.5419

Table 2. Search.conv 'within state' on topographic data. (θ represents the average phenotypic angle between species sharing the same dietary category. θ_{time} corresponds to the angular distance divided by the patristic distance between species. p indicates p-value, p_{FDR} refers to Benjamini–Hochberg adjusted p-values.)

diet category	n	θ	$p(\theta)$	$p_{FDR}(\theta)$	θ_{time}	$p(\theta_{time})$	$p_{FDR}(\theta_{time})$
frugivorous	7	58.914	0.0145	0.0386	0.669	0.0056	0.0448
herbivorous	4	17.925	0.0008	0.0064	0.517	0.0145	0.0582
hypercarnivorous	54	85.315	0.1478	0.2951	1.271	0.7295	0.9587
insectivorous	13	85.558	0.2394	0.3192	1.327	0.8225	0.9587
mesocarnivorous	11	93.571	0.6445	0.6445	1.601	0.9586	0.9587
molluscivorous	4	98.483	0.5991	0.6445	1.874	0.9445	0.9587
omnivorous	28	79.835	0.0060	0.0240	1.276	0.8310	0.9587
piscivorous	8	79.832	0.1844	0.2950	1.278	0.7384	0.9559

while more impactful in topography (see the electronic supplementary material, tables S1 and S2). Whereas all significant convergence results remained qualitatively equal, and often quantitatively similar, the corresponding results in topography were notably different. Remarkably, hypercarnivorous taxa were identified as topographically convergent only when body mass explained variance was retrieved, suggesting that allometry may obscure similar topographic adaptations in these carnivorans. Despite this, the effect size of body mass on geometric data ($\xi^2 = 0.3163$) is superior to its impact on topography ($\xi^2 = 0.157$). However, body mass is not uncorrelated with phylogeny, nor is it with diet [11]. More trivially, the higher quantity of data generated by HD3GM methods compared with the topographic approach certainly helps in recovering ecomorphological signals. Furthermore, though topographic and occlusal complexity metrics capture objective anatomical features, they eventually produce a single value (often mean or sum) per taxon. Similar scalar values can consequently describe markedly distinct morphologies (figure 3), further eroding connection with the functional signal. This many-to-one topography induces functional signal dilution that certainly plays a role in the better explanatory power of trophic classification regarding geometry. When combining topographic data with fixed landmarks to see if gross geometrical description substantially improved diagnostic power, the effect size only grew from 3% ($\xi^2 = 0.054$–0.086; see the electronic supplementary material, table S6). Although the fixed landmarks used in our protocol were not designed to be self-sufficient (i.e. without semi-landmarks), this still suggests that a denser geometrical cover leads to significant increase in explanatory capabilities. Altogether, these considerations suggest that the association of scalar values, as obtained with topographic approach, with ecological traits can be challenging in datasets with extensive morphological disparity like carnassial crown shapes. Additionally, pragmatic concerns are also at play; occlusal complexity metrics such as OPCr and DNE are known to be notably affected by several processing steps, including smoothing [7,41,42]. This is especially problematic in large-scale analyses in which a certain trade-off between taxonomic coverage and model quality is often needed. This probably results in artificial lowering of topographic metrics' variance, and thus, quality of functional inference. Considering the distinct outcomes conveyed by both approaches, we recommend using topographic and crown complexity analyses to compare geometrically similar shapes; whether among closely related species or similar analogical structures. Law *et al.* [43] showed that morphological evolution at the infra- and interfamily levels is hierarchically structured. In this case, secondary variation of occlusal topography might be preferentially studied at the infrafamilial level. Therefore, we postulate that geometrical approaches—including high-density methods—are more robust at large taxonomic scales and recommend that topographic approaches should be restricted to high-quality meshes and to lower taxonomic levels. Hopkins *et al.* [44] demonstrated that controlling for phylogenetic information in dietary prediction analyses does not systematically enhance predictive performance and may, under certain conditions, be counterproductive. Indeed, evolutionary history is a key predictor of ecology in mammals; our analyses support this interpretation by recovering both high level of dietary explained variance and strong phylogenetic signal in carnassial tooth shape. The effect of phylogeny may depend on the characteristics of the studied material and the analytical framework. In particular, methodological tools and taxonomic

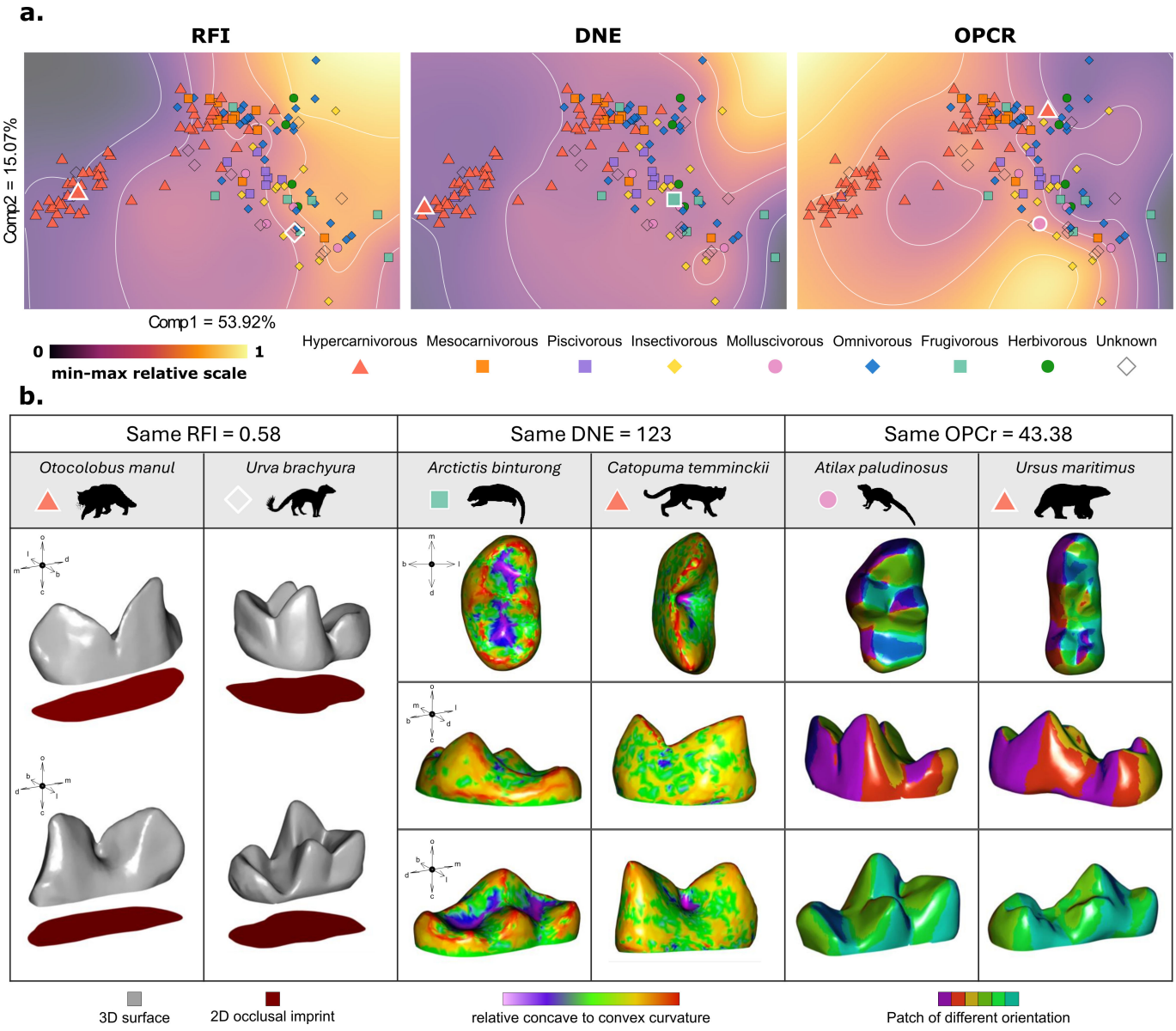

Figure 3. (a) Adaptative landscape of relative RFI, DNE and OPCr values. (b) Examples of distinct morphologies bearing similar topographic values. Axis system: o, occlusal; c, cervical; d, distal; m, mesial; b, buccal; l, lingual. Silhouettes from www.phylopic.org.

context may account for the observed outcomes [18]. Using phylogenetic structure in dental data may improve confidence in ecomorphological inference, but challenges remain for stem taxa and those with a preponderance of plesiomorphic or unspecialized features. More work specifically on early-diverging and transitional groups is needed to further clarify patterns in these taxa.

(b) Phenotypic parallelism and ecomorphology

Patterns congruent with within-diet convergence recovered by our analyses further demonstrate how fine-scale geometry captures functionally meaningful variation that is partly overlooked in topography. Whereas most dietary strategies occupy a relatively continuous morphospace, hypercarnivorous taxa diverge into two very distinct architectural solutions. This divergence exemplifies a case of many-to-one mapping [45] in the lower carnassial. As one morphotype is mostly associated with feliforms and the other with caniform carnivorans, we define those two morphotypes as 'felimorph' and 'canimorph' configurations. Both exhibit pronounced protoconid and paraconid development with strong proximo-distal orientation, transforming the tooth into an effective shearing blade. They mainly differ by the extreme reduction—or the total loss—of the metaconid and talonid in most felimorphs. This hypercarnassial architecture is found in most carnivorous feliforms as well as in many extinct clades such as hyaenodonts and nimravids [4]. Some caniforms, such as hypercarnivorous mustelids, also exhibit a specialized carnassial with no metaconid but displaying a blade-like talonid—the 'trenchant heel' *sensu* Lang & Martin [14]. These distinct architectures probably reflect constrained functional optima forcing convergence but only within each taxonomic frame, potentially explaining why no clear convergence signal is recovered at the scale of the entire dietary category. By contrast, omnivory represents a broad ecomorphological category encompassing a wide range of feeding strategies [46], which probably contributes to the dilution of convergence signals although still significant in geometry ($p_{\mathrm{FDR}}(\theta_{\mathrm{time}}) = 0.0012$). Omnivorous carnivorans generally retain a complete, functional trigonid combined with a well-developed talonid, producing a widened and

elongated carnassial morphology. Additionally, such taxa often evolved neomorph structures (i.e. crests and cusps) leading to extended disparity. However, omnivorous species are widespread across the carnivoran phylogeny, except in a few specialized clades (e.g. Felidae). As a result, even modest geometric similarity can accumulate into a statistically detectable convergence signal. Insectivorous carnivorans exhibit a more pronounced geometric resemblance, often characterized by triangular trigonids and relatively low but expanded talonids, sometimes reminiscent of early carnivoramorphans morphologies. Interestingly, the convergence signal in this group is partly mediated by body mass (see the electronic supplementary material, S6), suggesting that allometric constraints may interact with functional demands to shape their dental morphology [16,32]. Finally, frugivorous carnivorans provide a clear example of recurrent morphological transformation towards enlarged talonids and relatively low trigonids. While this diet is uncommon in Carnivora, the recurrence of this similar architecture across most frugivores suggests divergent mechanical demand [7], resulting in convergence detectable in both geometry ($p_{FDR}(\theta_{time}) = 0.0019$) and, uniquely, occlusal topography ($p_{FDR}(\theta_{time}) = 0.0344$).

(c) Dense geometry insights in future ecological and evolutionary studies

HD3DGM was developed to efficiently capture fine scale morphological variation and/or quantify the shape of structures lacking homologous landmarks [47–49]. Fischer *et al*. [32] introduced a semi-automated protocol designed for biological objects with a rather simple architecture (i.e. teeth in marine amniotes, belemnite guards, iguanodontian pollex, all of which are usually conical) that relies on very little pre-processing labour and is therefore faster to implement than previous pipelines. Since then, it has been successfully applied to quantify the shape of a wider variety of objects such as fish otoliths [50], squamate osteoderms [51] or intercheliceral sclerites in spiders [52]. In essence, this method can be applied to most biological items, but its use in morphologically disparate datasets remains challenging as a single template must accommodate for the entirety of studied shapes. Whereas the initial workflow consisted of dense but random sampling of the template surface, our revised approach differs by, first, using geodesic distance maximization to homogenize the distribution of the sampled template vertices and, second, sampling the desired number of pseudolandmarks by extracting coordinates whose distance between one-another is maximized (figure 1a.2). This results in uniform and relief-dependent sampling of the template, which then better accommodates the surfaces where the pseudolandmarks are projected. This expands the disparity and complexity of shapes that can be assessed without compromising the method's ease of use.

In highly disparate datasets, the choice of a simple template is usually recommended [53]. After extensive testing, we found that an early Carnivoraform carnassial tooth was the most efficient to obtain minimal distribution inequities when projecting the surface pseudolandmarks on each model. This tooth, which resembles the one exhibited by the common ancestor of the order Carnivora [54], is not close to the average shape of the extant species' morphospace. Our tests suggest that using the ancestral rather than mean shape as the template produces more homogenous pseudolandmarks cover on highly derived carnivoran teeth. Whereas substantiating this hypothesis would require dedicated methodological and statistical testing, it may be worth considering if the ability of this plesiomorphic carnassial morphology to serve as an efficient template—readily deformable to accommodate the wide range of dental morphologies in this dataset—could mirror underlying evolutionary constraints and differential permittivity in the morphological evolution of the various loci of this tooth. Following this hypothesis, a plesiomorph template might represent a particularly flexible configuration from which the diversity of subsequent morphologies can be derived. Phenotypic evolution may not occur within a flat Euclidean space but rather along curved, non-Euclidean manifolds [55,56]. Under such a framework, apparent centrality within a Euclidean morphospace may partly reflect projection artefacts rather than evolutionary proximity. In this context, it can be hypothesized that plesiomorphic morphologies occupy regions of the manifold with higher geodesic connectivity, potentially making them particularly effective templates for accommodating a wide range of derived forms.

Ethics. This work did not require ethical approval from a human subject or animal welfare committee.

Data accessibility. All data, code and information can be found in OSF [57].

Supplementary material is available online [58].

Declaration of AI use. We have not used AI-assisted technologies in creating this article.

Authors' contributions. M.V.: conceptualization, data curation, formal analysis, funding acquisition, investigation, methodology, project administration, visualization, writing—original draft; V.F.: conceptualization, funding acquisition, investigation, methodology, project administration, resources, supervision, writing—original draft; M.M.: data curation, methodology, writing—original draft; D.T.: data curation, methodology, writing—original draft; T.I.P.: visualization, writing—original draft; C.M.: methodology, supervision, writing—original draft; Z.J.T.: funding acquisition, methodology, supervision, writing—original draft; N.C.: conceptualization, data curation, funding acquisition, investigation, methodology, project administration, supervision, visualization, writing—original draft.

All authors gave final approval for publication and agreed to be held accountable for the work performed therein.

Conflict of interest declaration. We declare we have no competing interests.

Funding. We gratefully acknowledge the financial support that made this project possible. Specifically, we thank the following funding bodies and programs: Fonds de la Recherche Scientifique (F.R.S.–FNRS), grant FRIA FC 63999 (M.V.). Labex BCDiv (ANR-10-LABX-0003) and the Fondation Fyssen (M.M.). Doctoral School ED 227 "Sciences de la nature et de l'homme: évolution et écologie" (M.M.). Italian Ministry of University and Research, PNRR, Mission 4 Component 2, "Dalla ricerca all'impresa", Investment 1.4, Project CN00000033 (D.T.). Leverhulme Trust Early Career Research Fellowship (grant no. ECF-2025-468) (T.I.P.). Belgian American Educational Foundation (BAEF) Fellowship (N.C.). National Science Foundation, grant NSF DBI-2128146 (N.C., Z.J.T.).

Acknowledgements. We are extremely thankful to all the researchers, curators, collection managers and staff, whose help and support was fundamental to collect all the scans we needed to perform this study. Especially, we would like to thank: Thierry Smith, for his meaningful help and guidance. For access to the specimens that allowed us to complete this project we are immensely grateful to all the curatorial staff of the institutions we visited, more specifically Annelise Folie and Olivier Pauwels (RBINS, Brussels, Belgium), Emmanuel Gilissen (RMCA, Tervuren, Belgium), Geraldine Véron (MNHN, Paris, France), Daniela Kalthoff and Thomas Mörs (NRM, Stockholm, Sweden), Chris J. Conroy

(MVZ, Berkley, USA). For providing us additional scans, we would like to thank all the institutions and individuals who made scans available on various platform, more precisely Alejandro Pérez-Ramos, the Florida field museum, the University of Florida, Museu de Ciències Naturals de Barcelona, University of California Los Angeles and the American Museum of Natural History as well as all the staff behind MorphoSource, Sketchfab and Digimorph.

References

1. Berkovitz BKB, Shellis RP. 2018 *The teeth of mammalian vertebrates*. Amsterdam, The Netherlands; New York, NY: Academic Press/Elsevier.
2. Pineda-Munoz S, Lazagabaster IA, Alroy J, Evans AR. 2017 Inferring diet from dental morphology in terrestrial mammals. *Methods Ecol. Evol.* **8**, 481–491. (doi:10.1111/2041-210X.12691)
3. Peterkova R, Lesot H, Peterka M. 2006 Phylogenetic memory of developing mammalian dentition. *J. Exp. Zool. B Mol. Dev. Evol.* **306**, 234–250. (doi:10.1002/jez.b.21093)
4. Van Valkenburgh B. 2007 Deja vu: the evolution of feeding morphologies in the Carnivora. *Integr. Comp. Biol.* **47**, 147–163. (doi:10.1093/icb/icm016)
5. Crofts SB, Smith SM, Anderson PSL. 2020 Beyond description: the many facets of dental biomechanics. *Integr. Comp. Biol.* **60**, 594–607. (doi:10.1093/icb/icaa103)
6. Pollock TI, Hocking DP, Evans AR. 2022 The killer's toolkit: remarkable adaptations in the canine teeth of mammalian carnivores. *Zool. J. Linn. Soc.* **196**, 1138–1155. (doi:10.1093/zoolinnean/zlab064)
7. Berthaume MA, Lazzari V, Guy F. 2020 The landscape of tooth shape: over 20 years of dental topography in primates. *Evol. Anthropol.* **29**, 245–262. (doi:10.1002/evan.21856)
8. Gómez-Robles A, Polly PD. 2012 Morphological integration in the hominin dentition: evolutionary, developmental, and functional factors: morphological integration in the hominin dentition. *Evolution (N Y)* **66**, 1024–1043. (doi:10.1111/j.1558-5646.2011.01508.x)
9. Lang AJ, Engler T, Martin T. 2022 Dental topographic and three-dimensional geometric morphometric analysis of carnassialization in different clades of carnivorous mammals (Dasyuromorphia, Carnivora, Hyaenodonta). *J. Morphol.* **283**, 91–108. (doi:10.1002/jmor.21429)
10. Werdelin L. 1996 Community-wide character displacement in Miocene hyaenas. *Lethaia* **29**, 97–106. (doi:10.1111/j.1502-3931.1996.tb01843.x)
11. Gittleman JL. 1986 Carnivore life history patterns: allometric, phylogenetic, and ecological associations. *Am. Nat.* **127**, 744–771. (doi:10.1086/284523)
12. Meloro C, Raia P. 2010 Cats and dogs down the tree: the tempo and mode of evolution in the lower carnassial of fossil and living carnivora. *Evol. Biol.* **37**, 177–186. (doi:10.1007/s11692-010-9094-3)
13. James Rohlf F, Marcus LF. 1993 A revolution morphometrics. *Trends Ecol. Evol. (Amst.)* **8**, 129–132. (doi:10.1016/0169-5347(93)90024-J)
14. Lang AJ, Martin T. 2024 Hypoflexid function in the 'trenchant heel' of carnassial teeth, with comments on talonid evolution. *Mamm. Res.* **69**, 533–548. (doi:10.1007/s13364-024-00762-1)
15. Crusafont-Pairó M, Truyols-Santonja J. 1956 A biometric study of the evolution of fissiped carnivores. *Evolution (N Y)* **10**, 314–332. (doi:10.1111/j.1558-5646.1956.tb02855.x)
16. Tarquini SD, Chemisquy MA, Prevosti FJ. 2020 Evolution of the carnassial in living mammalian carnivores (Carnivora, Didelphimorphia, Dasyuromorphia): diet, phylogeny, and allometry. *J. Mammal. Evol.* **27**, 95–109. (doi:10.1007/s10914-018-9448-7)
17. Evans AR, Wilson GP, Fortelius M, Jernvall J. 2007 High-level similarity of dentitions in carnivorans and rodents. *Nature* **445**, 78–81. (doi:10.1038/nature05433)
18. Waldman E, Gonzalez Y, Flynn JJ, Tseng ZJ. 2023 Dental topographic proxies for ecological characteristics in carnivoran mammals. *J. Anat.* **242**, 627–641. (doi:10.1111/joa.13806)
19. Castiglione S *et al*. 2019 A new, fast method to search for morphological convergence with shape data. *PLoS ONE* **14**, e0226949. (doi:10.1371/journal.pone.0226949)
20. Goswami A, Milne N, Wroe S. 2011 Biting through constraints: cranial morphology, disparity and convergence across living and fossil carnivorous mammals. *Proc. R. Soc. B* **278**, 1831–1839. (doi:10.1098/rspb.2010.2031)
21. Meloro C, Clauss M, Raia P. 2015 Ecomorphology of carnivora challenges convergent evolution. *Org. Divers. Evol.* **15**, 711–720. (doi:10.1007/s13127-015-0227-5)
22. Meloro C, O'Higgins P. 2011 Ecological adaptations of mandibular form in fissiped carnivora. *J. Mammal. Evol.* **18**, 185–200. (doi:10.1007/s10914-011-9156-z)
23. Tamagnini D, Meloro C, Raia P, Maiorano L. 2021 Testing the occurrence of convergence in the craniomandibular shape evolution of living carnivorans. *Evolution (N Y)* **75**, 1738–1752. (doi:10.1111/evo.14229)
24. Tseng ZJ, Wang X. 2011 Do convergent ecomorphs evolve through convergent morphological pathways? Cranial shape evolution in fossil hyaenids and borophagine canids (Carnivora, Mammalia). *Paleobiology* **37**, 470–489. (doi:10.1666/10007.1)
25. Wroe S, Milne N. 2007 Convergence and remarkably consistent constraint in the evolution of carnivore skull shape. *Evolution (N Y)* **61**, 1251–1260. (doi:10.1111/j.1558-5646.2007.00101.x)
26. Chatar N, Michaud M, Tamagnini D, Fischer V. 2024 Evolutionary patterns of cat-like carnivorans unveil drivers of the sabertooth morphology. *Curr. Biol.* **34**, 2460–2473. (doi:10.1016/j.cub.2024.04.055)
27. Burgin CJ, Colella JP, Kahn PL, Upham NS. 2018 How many species of mammals are there? *J. Mammal.* **99**, 1–14. (doi:10.1093/jmammal/gyx147)
28. Faurby S, Morlo M, Werdelin L. 2021 CarniFOSS: a database of the body mass of fossil carnivores. *Global Ecol. Biogeogr.* **30**, 1958–1964. (doi:10.1111/geb.13369)
29. Faurby S, Silvestro D, Werdelin L, Antonelli A. 2024 Reliable biogeography requires fossils: insights from a new species-level phylogeny of extinct and living carnivores. *Proc. R. Soc. B* **291**, 20240473. (doi:10.1098/rspb.2024.0473)
30. Schliep KP. 2011 phangorn: phylogenetic analysis in R. *Bioinformatics* **27**, 592–593. (doi:10.1093/bioinformatics/btq706)
31. Boyer DM. 2008 Relief index of second mandibular molars is a correlate of diet among prosimian primates and other euarchontan mammals. *J. Hum. Evol.* **55**, 1118–1137. (doi:10.1016/j.jhevol.2008.08.002)
32. Fischer V, Bennion RF, Foffa D, MacLaren JA, McCurry MR, Melstrom KM, Bardet N. 2022 Ecological signal in the size and shape of marine amniote teeth. *Proc. R. Soc. B* **289**, 20221214. (doi:10.1098/rspb.2022.1214)
33. Schlager S. 2017 Morpho and Rvcg – shape analysis in R. In *Statistical shape and deformation analysis*, pp. 217–256. San Diego, CA: Academic Press/Elsevier. (doi:10.1016/B978-0-12-810493-4.00011-0)
34. Adams DC, Otárola-Castillo E. 2013 geomorph: an R package for the collection and analysis of geometric morphometric shape data. *Methods Ecol. Evol.* **4**, 393–399. (doi:10.1111/2041-210X.12035)
35. Pampush JD, Winchester JM, Morse PE, Vining AQ, Boyer DM, Kay RF. 2016 Introducing molaR: a new R package for quantitative topographic analysis of teeth (and other topographic surfaces). *J. Mammal. Evol.* **23**, 397–412. (doi:10.1007/s10914-016-9326-0)

36. Bunn JM, Boyer DM, Lipman Y, St Clair EM, Jernvall J, Daubechies I. 2011 Comparing Dirichlet normal surface energy of tooth crowns, a new technique of molar shape quantification for dietary inference, with previous methods in isolation and in combination. *Am. J. Phys. Anthropol.* **145**, 247–261. (doi:10.1002/ajpa.21489)
37. Clavel J, Escarguel G, Merceron G. 2015 mv morph: an R package for fitting multivariate evolutionary models to morphometric data. *Methods Ecol. Evol.* (doi:10.1111/2041-210X.12420)
38. Guillerme T. 2018 dispRity: a modular R package for measuring disparity. *Methods Ecol. Evol.* **9**, 1755–1763. (doi:10.1111/2041-210X.13022)
39. Tung Ho L si, Ané C. 2014 A linear-time algorithm for Gaussian and non-Gaussian trait evolution models. *Syst. Biol.* **63**, 397–408. (doi:10.1093/sysbio/syu005)
40. Grossnickle DM, Brightly WH, Weaver LN, Stanchak KE, Roston RA, Pevsner SK, Stayton CT, Polly PD, Law CJ. 2024 Challenges and advances in measuring phenotypic convergence. *Evolution (N Y)* **78**, 1355–1371. (doi:10.1093/evolut/qpae081)
41. Evans AR, Janis CM. 2014 The evolution of high dental complexity in the horse lineage. *Ann. Zool. Fenn.* **51**, 73–79. (doi:10.5735/086.051.0209)
42. Ungar PS, M'Kirera F. 2003 A solution to the worn tooth conundrum in primate functional anatomy. *Proc. Natl Acad. Sci. USA* **100**, 3874–3877. (doi:10.1073/pnas.0637016100)
43. Law CJ, Hlusko LJ, Tseng ZJ. 2025 Long-fuse evolution of carnivoran skeletal phenomes through the Cenozoic. *Proc. R. Soc. B* **292**, 20252400. (doi:10.1098/rspb.2025.2400)
44. Hopkins SSB, Price SA, Chiono AJ. 2022 Influence of phylogeny on the estimation of diet from dental morphology in the Carnivora. *Paleobiology* **48**, 324–339. (doi:10.1017/pab.2021.37)
45. Chatar N, Fischer V, Tseng ZJ. 2022 Many-to-one function of cat-like mandibles highlights a continuum of sabre-tooth adaptations. *Proc. R. Soc. B* **289**, 20221627. (doi:10.1098/rspb.2022.1627)
46. Pineda-Munoz S, Alroy J. 2014 Dietary characterization of terrestrial mammals. *Proc. R. Soc. B* **281**, 20141173. (doi:10.1098/rspb.2014.1173)
47. Alfieri F, Botton-Divet L, Wölfer J, Nyakatura JA, Amson E. 2023 A macroevolutionary common-garden experiment reveals differentially evolvable bone organization levels in slow arboreal mammals. *Commun. Biol.* **6**, 995. (doi:10.1038/s42003-023-05371-3)
48. Bardua C, Fabre AC, Clavel J, Bon M, Das K, Stanley EL, Blackburn DC, Goswami A. 2021 Size, microhabitat, and loss of larval feeding drive cranial diversification in frogs. *Nat. Commun.* **12**, 2503. (doi:10.1038/s41467-021-22792-y)
49. Goswami A, Watanabe A, Felice RN, Bardua C, Fabre AC, Polly PD. 2019 High-density morphometric analysis of shape and integration: the good, the bad, and the not-really-a-problem. *Integr. Comp. Biol.* **59**, 669–683. (doi:10.1093/icb/icz120)
50. Van Damme A, Huet E, Frédérich B, Parmentier E. 2025 The influence of habitat complexity on otolith morphology and sensory capacities in Nile tilapia: a controlled experimental approach. *J. Exp. Biol.* **228**, JEB249693. (doi:10.1242/jeb.249693)
51. Annear E, Van Linden L, MacLaren JA, Baeckens S, Broeckhoven C, Van Damme R. 2025 Intraspecific variation in osteoderm morphology in a cordylid lizard. *Zool. J. Linn. Soc.* **205**, zlaf184. (doi:10.1093/zoolinnean/zlaf184)
52. Black CR, Shultz JW, Wood HM. 2025 Extended phenotype affects somatic phenotype in spiders: web builders have lower estimated biting forces than free hunters. *Evolution (N Y)* **79**, 380–392. (doi:10.1093/evolut/qpae170)
53. Souter T, Cornette R, Pedraza J, Hutchinson J, Baylac M. 2010 Two applications of 3D semi-landmark morphometrics implying different template designs: the theropod pelvis and the shrew skull. *Comptes Rendus Palevol.* **9**, 411–422. (doi:10.1016/j.crpv.2010.09.002)
54. Smith T, Smith R. 2010 A new genus of 'Miacid' carnivoran from the earliest Eocene of Europe and North America. *Acta Palaeontol. Pol.* **55**, 761–764. (doi:10.4202/app.2009.0125)
55. Kendall DG. 1977 The diffusion of shape. *Adv. Appl. Probab.* **9**, 428–430. (doi:10.2307/1426091)
56. Boyko JD, Rabosky DL. 2026 The geometry of macroevolution: phenotypic evolution on non-euclidean manifolds. *Am. Nat.* **207**, 751–762. (doi:10.1086/740145)
57. Vankelst M, Fischer V. 2026 Data for: Decoupling geometry and topography reveals contrasting ecomorphological signals in carnivoran carnassial teeth. OSF (doi:10.17605/OSF.IO/7JW5X)
58. Vankelst M *et al*. 2026 Supplementary material from: Decoupling geometry and topography reveals contrasting ecomorphological signals in carnivoran carnassial teeth. Figshare. (doi:10.6084/m9.figshare.c.8555994)